CMI

www.nature.com/cmi

ARTICLE

Check for updates

Extracellular nucleoprotein exacerbates influenza virus pathogenesis by activating Toll-like receptor 4 and the NLRP3 inflammasome

Chang-Ung Kim[1,2], Yu-Jin Jeong[3], Pureum Lee[3,4], Moo-Seung Lee[3,4], Jong-Hwan Park[5], Young-Sang Kim[2]✉ and Doo-Jin Kim[1,2,4]✉

Host immune responses, such as those initiated by pattern recognition receptor (PRR) activation, are important for viral clearance and pathogenesis. However, little is known about the interactions of viral proteins with surface PRRs or, more importantly, the association of innate immune activation with viral pathogenesis. In this study, we showed that internal influenza virus proteins were released from infected cells. Among these proteins, nucleoprotein (NP) played a critical role in viral pathogenesis by stimulating neighboring cells through toll-like receptor (TLR)2, TLR4, and the NLR family pyrin domain containing 3 (NLRP3) inflammasome. Through the activation of these PRRs, NP induced the production of interleukin (IL)-1β and IL-6, which subsequently led to the induction of trypsin. Trypsin induced by NP increased the infectivity of influenza virus, leading to increases in viral replication and pathology upon subsequent viral infection. These results reveal the role of released NP in influenza pathogenesis and highlight the importance of the interactions of internal viral proteins with PRRs in the extracellular compartment during viral pathogenesis.

Keywords: Influenza virus; Viral protein release; Nucleoprotein; Toll-like receptor; Cyotkine-trypsin cycle

Cellular & Molecular Immunology (2022) 19:715–725; https://doi.org/10.1038/s41423-022-00862-5

INTRODUCTION

Influenza is a major global health problem, causing approximately 3–5 million cases of severe illness and 290000–650000 deaths annually. Although several vaccines and therapeutic agents are commercially available, frequent antigenic changes might render them less effective or inapplicable [1]. Therefore, understanding the mechanisms of viral pathogenesis is required for the development of novel antiviral approaches.

Pattern recognition receptors (PRRs) are the first line of defense of the host innate immune system, which provides immediate protection against infectious pathogens. PRRs recognize pathogen-associated molecular patterns (PAMPs) and trigger the activation of responses by the innate immune system, such as the production of antiviral and proinflammatory cytokines/chemokines and subsequent infiltration of immune cells to the infection site [2]. These are critical events for viral clearance. For example, activation of Toll-like receptor (TLR)3, retinoic-acid inducible gene I (RIG-I), and mitochondrial antiviral-signaling protein (MAVS) by influenza virus RNA leads to the production of type I interferons (IFNs), which are critical factors for antiviral immunity during the initial stage of infection [3].

PRR activation, however, often results in increased viral pathogenesis. Influenza virus proteins such as PB1-F2 and M2 increase viral pathogenesis through the activation of the NLR family pyrin domain containing 3 (NLRP3) inflammasome [4, 5]. In addition, surface glycoproteins of dengue virus, Ebola virus, and vesicular stomatitis virus are known to directly interact with TLR4, leading to virus-induced inflammation [6–8]. Intriguingly, a recent study showed that the spike protein of SARS-CoV-2 is sensed by TLR2 to induce inflammatory cytokine production [9]. Therefore, further investigation into the interactions between viral proteins and host PRRs is imperative for understanding the mechanisms of viral pathogenesis and developing novel therapeutic measures.

In this study, we investigated the role of influenza virus proteins in viral pathogenesis mediated via PRR activation in a mouse model. The release of nucleoprotein (NP) from infected cells triggered innate immune activation via a direct interaction with TLR4 on monocytic cells. These results suggest a pathogenic role for NP in influenza virus pathogenesis and a new perspective on the interaction mode between internal viral proteins and PRRs on neighboring cells in the extracellular compartment.

[1]Infectious Disease Research Center, Korea Research Institute of Bioscience and Biotechnology (KRIBB), Daejeon, South Korea. [2]Department of Biochemistry, Chungnam National University, Daejeon, South Korea. [3]Environmental Diseases Research Center, Korea Research Institute of Bioscience and Biotechnology (KRIBB), Daejeon, South Korea. [4]University of Science and Technology (UST), Daejeon, South Korea. [5]College of Veterinary Medicine, Chonnam National University, Gwangju, South Korea. ✉email: young@cnu.ac.kr; golddj@kribb.re.kr

Received: 1 October 2021 Accepted: 20 March 2022
Published online: 22 April 2022

MATERIALS AND METHODS

Mice

Seven- to eight-week-old female C57BL/6 mice were purchased from KOATECH (Gyeonggi-do, Korea) and maintained in a specific pathogen-free, biosafety level-2 facility at the Korea Research Institute of Bioscience and Biotechnology (KRIBB). TLR2 KO and TLR4 KO mice were purchased from The Jackson Laboratory, and TLR2/4 DKO mice were generated by breeding TLR2 KO and TLR4 KO mice. NLRP3 KO and caspase-1/11 KO mice were obtained from Prof. Gabriel Nuñez at the University of Michigan (USA). MyD88 KO and TRIF KO mice were obtained from Profs. Sin-Hyeog Im and Kwang Soon Kim at POSTECH (Korea). In this study, only female mice were used, and the mice were 8–12 weeks old. All animal experiments were approved by the Institutional Animal Use and Care Committee of the KRIBB and performed in accordance with the Guide for the Care and Use of Laboratory Animals published by the U.S. National Institutes of Health.

Cell culture

THP-1 cells were purchased from ATCC and maintained in Roswell Park Memorial Institute (RPMI) 1640 medium (Corning, NY, USA) supplemented with 10% fetal bovine serum (FBS; HyClone, Logan, Utah, USA) and 1× antibiotics (Gibco, Massachusetts, USA). HEK Blue TLR (InvivoGen, San Diego, CA, USA), L929 (ATCC), MDCK (ATCC), and A549 (ATCC) cells were maintained in Dulbecco's modified Eagle's medium (DMEM, Corning) supplemented with 10% FBS (HyClone) and 1× antibiotics (Gibco). BMDMs were generated from C57BL/6 N, TLR2 KO, TLR4 KO, TLR2/4 DKO, NLRP3 KO, caspase-1/11 DKO, MyD88 KO, and TRIF KO mice. For the preparation of BMDMs, bone marrow cells were harvested from the femur and tibia and differentiated in DMEM (Corning) containing 25% L929-conditioned medium, 10% FBS (HyClone), and 1× antibiotics (Gibco). L929 cells were grown until confluent in DMEM containing 10% FBS (HyClone) and 1× antibiotics (Gibco). The medium was changed, and the cells were incubated for 7 days, after which the supernatants were harvested and filtered. Cells were cultured at 37 °C with 5% CO_2.

Virus

The influenza A/Puerto Rico/8/1934 (PR8) virus was cultivated in the allantoic cavities of embryonated chicken eggs. Viruses were titrated by calculating the 50% egg infectious dose (EID_{50}) and 50% tissue culture infective dose ($TCID_{50}$) and stored at −80 °C until use.

Plasmid DNA cloning for immunization and protein expression

Recombinant DNA was used for mouse immunization. For protein expression and purification, DNA fragments suitable for cloning of NP and the R416A mutant were cloned into pEXPR-IBA 103 vectors (IBA Lifesciences, Göttingen, Germany). Recombinant plasmid DNA expressing NP, M1, PA, PB1, PB2, NS1, NS2, and PB1-F2 was constructed in the DNA vector pGX-10. pGX-10 is a DNA vaccine vector composed of a CMV promoter, a tripartite leader sequence, a late poly A signal sequence of simian virus 40, a simian virus 40 enhancer, and a kanamycin resistance gene [10]. The NP, M1, PA, PB1, PB2, and NS1 genes were obtained from the PR8 virus, and the R416A mutant NP, NS2, and PB1-F2 genes were synthesized by CosmogenTech (Seoul, Korea).

Protein purification

The pEXPR-IBA 103-NP plasmid was obtained using a maxi prep kit (QIAGEN, Hilden, Germany). DNA was transfected into ExpiCHO cells using a transfection system (Gibco), and enhancers and feeds were added 20 h after transfection (Gibco). After 5 days of transfection, the cells were centrifuged at 4000 rpm for 30 min, and the supernatant was removed. A 1× strep wash buffer (IBA Lifesciences) was added to the cells, sonication (58%, 10 s on/10 s off, total time: 10 min) was performed, and the supernatant was collected after centrifugation at 13,000 rpm for 30 min. After filtering the supernatant using a 0.45-μm filter (Corning), it was bound to strep-tactin XT resin (IBA Lifesciences) using a gravity flow column. After washing with 5 bed volumes of 1X wash buffer (IBA Lifesciences), the bound protein was eluted with elution buffer (IBA Lifesciences) . The endotoxin level in the purified protein sample was determined using an endotoxin test kit (Thermo Fisher Scientific, Waltham, Massachusetts, USA). Protein sample was stored at −80 °C until use.

Serum harvest and antibody purification

Mice were immunized intramuscularly with NP-, M1-, PA-, PB1-, PB2-, NS1-, NS2-, and PB1-F2-expressing plasmid DNA (10 μg) by electrophoresis. Mice were immunized twice, with a 3-week interval between the immunizations. Serum was obtained 2 weeks after the final vaccination. Anti-NP serum was purified from the serum of mock- or NP-vaccinated mice using an serum antibody purification kit (Abcam) according to the manufacturer's protocol. Serum and purified antibodies were stored at −20 °C.

Experimental schedule

Mice were infected intranasally with the PR8 virus. The immune cell population in the lungs and the levels of viral proteins in the BALF were determined at each indicated time point. To investigate the functions of the influenza virus-cytokine-trypsin cycle induced by NP, mice were infected with the PR8 virus (32 PFU) 3 days pre- and post-injection of PBS, NP, IL-1ß (R&D Systems, Minneapolis, Minnesota, USA), or IL-6 (R&D Systems) or infected with virus treated with trypsin. For serum transfer, 200 μl of anti-NP serum or purified serum IgG (200 μg) was injected into the intraperitoneal cavity daily for 3 days. NK cells were depleted by intraperitoneal injection of an anti-mouse NK1.1 antibody (100 μg/mouse, PK136; BioLegend). Two days after NK-cell depletion, mice were infected with influenza virus. The body weight change and survival rate of mice were monitored for 14 days after infection with influenza virus.

Lung and BALF sampling

Total lung samples were obtained at the indicated time points. Lungs were minced, and 1.5 ml of RPMI 1640 medium containing collagenase D (150 unit/ml, Gibco), DNase I (50 μg/ml, Merck, Kenilworth, New Jersey, USA), 10% FBS, and 1× antibiotics was added and incubated for 90 min. Then, 3 μl of 0.5 M EDTA was added to the mixture and allowed to react for 20 min. Cells were separated from the lung tissue using a strainer (SPL). The lung cells were treated with RBC lysis buffer (BD Biosciences) for RBC lysis. For BALF sampling, after euthanasia, the trachea was catheterized, and the BALF was collected by flushing the lungs twice with 1 ml of ice-cold PBS containing protease inhibitors (Merck). Cells were removed via centrifugation (4000 rpm, 5 min, 4 °C), and the BALF was obtained and stored at −80 °C.

Viral titration

MDCK cells were cultured in MEM containing 10% FBS and 1× antibiotics and seeded at 1×10^6 cells/well in a 6-well plate or 5×10^4 cells/well in a 96-well plate. After 16 h, the medium was removed, the cells were washed with PBS, and MEM containing 3.33 g/ml bovine serum albumin and 1× antibiotics was added. Influenza virus was treated with NP-treated BMDM culture supernatant with/without a protease inhibitor cocktail (Roche) at 37 °C for 1 h and then used to infect the cells for 1 h. After infection, the supernatant was removed, and the cells were washed with PBS and cultured in MEM containing 10% FBS (HyClone) and 1× antibiotics (Gibco). Three days after infection, the viral titer was determined with a hemagglutinin test and calculated by the Reed and Muench method. The viral titer is expressed as $\log_{10}$ of the 50% tissue culture infective dose ($TCID_{50}$) per milliliter. For qRT–PCR, total RNA was extracted from influenza virus-infected MDCK cells using an RNA prep kit (Clontech, California, USA). cDNA synthesis and RT–PCR were performed using the qRT–PCR Kit [Green] (NANOHELIX, Daejeon, Korea). *M* gene RT–PCR was performed. The fold difference in mRNA expression between treatment groups was determined by the standard delta-delta Ct method. GAPDH was used as an internal control.

Viral protein detection in the infected MDCK cell culture supernatant

MDCK or THP-1 cells were infected with the PR8 virus (10^3 $TCID_{50}$/ml), and A549 cells were infected with the PR8 virus (0.01 MOI) for 72 h. Subsequently, the cell culture supernatant was harvested by centrifugation (1500 rpm, 10 min, 4 °C) to remove cells from the culture supernatant. The cell culture supernatant was filtered using a 50-nm syringe filter. The influenza virus-infected MDCK cell culture supernatant was separated by sucrose gradient ultracentrifugation (sucrose 20–60%, 32000 rpm, 1 h, 4 °C). Viral proteins were detected in unfiltered, filtered, and ultracentrifuged samples using ELISA.

TLR reporter cell line assay

A TLR reporter cell line system that monitored TLR activity using secreted embryonic alkaline phosphatase (SEAP) induced by NF-κB and AP-1 activation was used. HEK-Blue™ Detection (InvivoGen) reacts with SEAP to turn the medium color purple/blue, and the color intensity can be measured with a spectrophotometer. The TLR reporter cell lines (InvivoGen) were cultured in DMEM containing 10% FBS and 1× antibiotics. When the cells reached 80% confluent, they were washed with PBS, and detection medium was added to harvest the cells using a scraper. Cells (5×10^4 cells/well; 180 µl) were seeded in a 96-well plate, and 20 µl of PBS, samples, PAM3 (Invitrogen, Waltham, Massachusetts, USA), LPS (Invitrogen), poly I:C (Invitrogen), flagellin (Invitrogen), R848 (Invitrogen), or CpG-ODN (Invitrogen) was added to each well. Then, the cells were cultured at 37 °C, 5% CO_2, and 90% humidity for 20 h, and the absorbance at 630 nm was recorded.

Flow cytometry

Single-lung-cell suspensions were blocked using anti-mouse CD16/CD32 (mouse BD Fc block, BD Biosciences, New Jersey, USA) at room temperature for 15 min prior to staining. Surface antigens were stained with the indicated conjugated antibodies at room temperature for 15 min. The following antibodies were used: APC-conjugated anti-CD4 (Thermo Fisher Scientific), PerCP-eFluor 710-conjugated anti-CD3e (Thermo Fisher Scientific), PE-Cyanine7-conjugated anti-CD45R (Thermo Fisher Scientific), APC/Cyanine7-conjugated anti-CD45 (BioLegend, San Diego, CA, USA), PE-conjugated anti-Siglec-F (Thermo Fisher Scientific), PerCD-eFluor710-conjugated anti-Ly6G, Alexa Fluor 700-conjugated anti-MHC Class II (I-A/I-E) (Thermo Fisher Scientific), eFluor 450-conjugated anti-F4/80 (Thermo Fisher Scientific), APC-conjugated anti-CD11b (BioLegend), FITC-conjugated anti-NK1.1 (BD Biosciences), PE-conjugated anti-CD49b (BioLegend), and PerCP-e710-conjugated anti-CD3e (BD Biosciences). For all experiments, cells were analyzed using a Gallios flow cytometer (Beckman Coulter). Panel setup and fluorescence compensation were performed using UltraCompeBeads™ Compensation Beads (Invitrogen). All analyses were performed using FlowJo software (Becton, Dickinson and Company, New Jersey, USA).

ELISA

BMDMs, A549 cells, and THP-1 cells were seeded at 1×10^6 cells/well, and the THP-1 cells were treated with a TLR4 inhibitor (Merck) or an NLRP3 inhibitor (InvivoGen) for 1 h. The cells were treated with purified NP, PAM3 (InvivoGen), LPS (InvivoGen), and ATP (Sigma-Aldrich, Burlington, MA, USA). The BMDMs were treated with 50-nm-filtered infected cell culture supernatant and anti-NP serum. At 20 h after treatment, the supernatant was collected. BALF samples were obtained from mice at the indicated time points. Cytokines were measured in cell culture supernatants and BALF samples with IL-1β (R&D Systems), IL-6 (R&D Systems), CCL2 (R&D Systems), RANTES (R&D Systems), keratinocyte chemoattractant (KC) (R&D Systems), and trypsin (MY BioSource, San Diego, USA) ELISA kits according to the manufacturer's protocol.

For the detection of interaction between NP and TLRs, TLR2 (LSBio) and TLR4 (LSBio) proteins were used to coat an ELISA plate (Corning) at a concentration of 2 µg/mL (50 µl/well). After an overnight incubation at 4 °C, blocking was performed using 3% skim milk. NP was added at a concentration of 6.25–100 µg/ml (with/without purified serum anti-NP IgG) and incubated at room temperature for 2 h. Subsequently, an anti-NP antibody (Abcam) was diluted at 1:200, and 50 µl/well was added for 1 h. Then, anti-mouse total IgG-HRP (Cell Signaling Technology, Danvers, Massachusetts, USA) was diluted at 1:5000, and 50 µl/well was added for 1 h. Thereafter, a colorimetric reaction was performed by adding 50 µl/well TMB solution and then 25 µl/well 0.5 N H_2SO_4. The absorbance at 450 nm was then recorded.

Western blotting and immunoprecipitation (IP)

MDCK cells were infected with the PR8 virus (10^1–10^3 $TCID_{50}$/ml). BMDMs, THP-1 cells, and A549 cells were treated with PBS, NP, or LPS. The cells were lysed in CETilysis buffer (TransLab) for 10 min on ice. Samples were diluted in 1× Sample Buffer (TransLab) and boiled for 10 min. The samples were fractionated by SDS-polyacrylamide gel electrophoresis (SDS–PAGE). The proteins were transferred to PVDF membranes (Merck). The membranes were blocked with 3% BSA (Gibco) in TBS with 0.5% Tween (TBS-T) for 1 h, after which the membranes were incubated with primary antibodies overnight at 4 °C. The membranes were then washed three times with TBS-T for 5 min and incubated with HRP-conjugated secondary antibodies (all diluted in 3% BSA in TBS with 0.5% Tween). The bound antibodies were visualized using Immobilon Forte Western HRP substrate (Merck) and imaged using EZ capture II (ATTO). Dynabeads (Invitrogen) were coated with the indicated antibodies according to the manufacturer's instructions.

BMDMs were seeded at 1×10^6 cells/well in 6-well plates. The BMDMs were treated with rNP (100 µg/ml) for 30 min. The cells were treated with CETi lysis buffer (TransLab) for 10 min on ice. The lysates were centrifuged, and the supernatants were transferred to fresh tubes containing antibody-coated Dynabeads (Invitrogen). IP was performed following the manufacturer's instructions (Invitrogen). Samples were analyzed by western blot analysis. The following antibodies were used: anti-TLR2 (Abcam), anti-TLR4 (Santa Cruz, Thermo Fisher Scientific), anti-influenza NP (Santa Cruz, Abcam), anti-phospho-SAPK/JNK (Cell Signaling Technology), anti-phospho-p44/42 MAPK (Cell Signaling Technology), anti-phospho-p38 MAPK (Cell Signaling Technology), anti-phospho-IkappaB (Cell Signaling Technology), anti-rabbit IkappaB-alpha (Cell Signaling Technology), anti-NF-kappaB p65 (Cell Signaling Technology), anti-NLRP3 (Cell Signaling Technology), anti-β-actin (Cell Signaling Technology), anti-caspase-1 (Enzo Life sciences, Farmingdale, New York, USA), anti-Strep-tag II (Abcam, Cambridge, UK), HRP-linked anti-mouse IgG (Cell Signaling Technology), and HRP-linked anti-rabbit IgG (Cell Signaling Technology).

RESULTS

Influenza virus proteins are released from infected cells into the extracellular compartment

During the pathogenesis of influenza virus infection, viral proteins as well as complete viral particles can be released into the extracellular space by lytic cell death because internal viral proteins are present in the cytoplasm or nucleus of the infected cells [11]. To investigate the functions of these extracellular viral proteins in viral replication and pathogenicity, first, the presence of viral proteins released from influenza virus-infected cells was analyzed in vitro.

MDCK cells were infected with the PR8 virus (10^3 $TCID_{50}$/ml), and the culture supernatant was filtered through a filter with a pore size of 50 nm to remove intact influenza virions, as the diameter of influenza virus ranges between 80 nm and 120 nm. Internal viral proteins of influenza virus were detected at similar levels in the unfiltered and filtered culture supernatants, but the level of the envelope protein hemagglutinin (HA) was decreased in the filtered supernatant (Fig. 1a). To check whether the filtered supernatant contained influenza virus, reinfection with the filtered supernatant was performed, and the $TCID_{50}$, M gene replication, and viral protein expression were not increased (Fig. 1b–d). Furthermore, the detection of NP among the internal viral proteins increased in an infectious dose-dependent manner (Fig. 1e). The release of internal viral proteins was further confirmed through classic viral purification. PR8 virus-infected MDCK cell culture supernatants were subjected to sucrose gradient ultracentrifugation for virus purification. After ultracentrifugation, the supernatant and sucrose were obtained by dividing the gradient into 4 fractions (Supplementary Fig. 1a). When each fraction was subjected to a $TCID_{50}$ assay, fraction 1 (supernatant fraction, referred to as #1) was observed to not contain the virus, while fraction 4 (sucrose fraction, referred to as #4) contained the virus (Supplementary Fig. 1b). Similar to the results obtained using a syringe filter, internal viral proteins were detected at similar levels in fractions #1 and #4 (Supplementary Fig. 1c and d), but the level of HA was significantly reduced in #1 (Supplementary Fig. 1d). These observations indicate that virion or cell-free internal proteins exist in the culture supernatant. Consistent with the in vitro data, viral proteins, including NP, M1, and NS1, were detected in the virion-free bronchoalveolar lavage fluid (BALF) of PR8-infected mice (Fig. 1f and Supplementary Fig. 1e). These data show that influenza virus proteins are released from infected cells and exist as virion-free entities in the extracellular compartment.

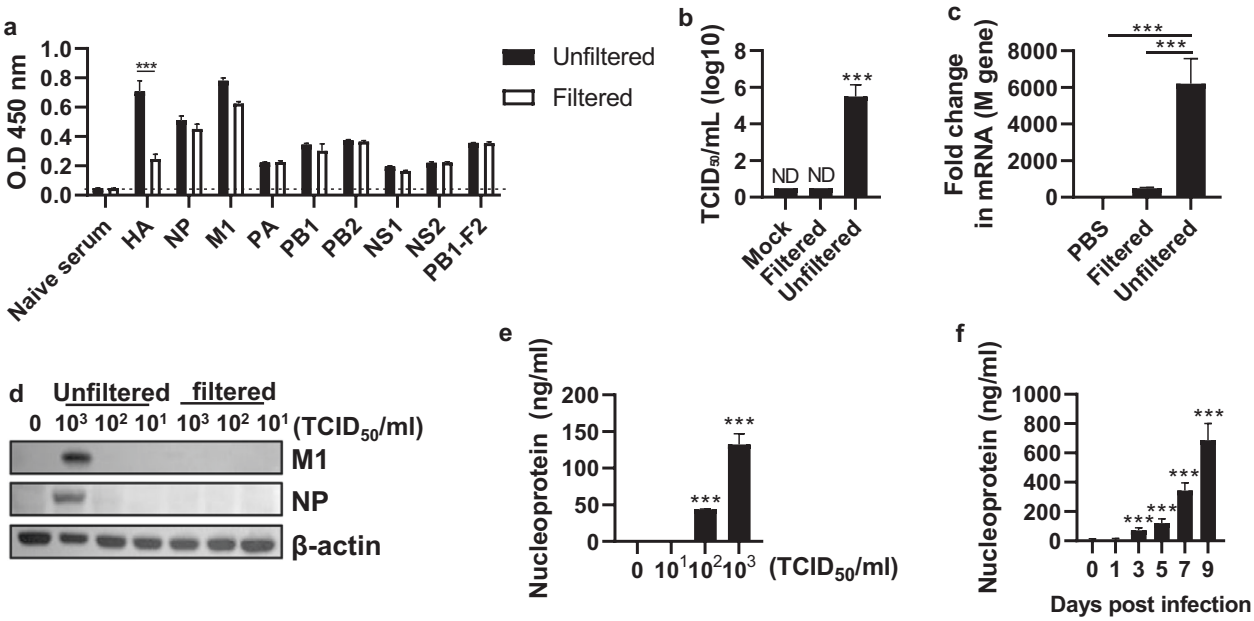

Fig. 1 Release of influenza virus proteins from influenza virus-infected cells MDCK cells were infected with the PR8 virus (10^3 $TCID_{50}$/ml) for 3 days, followed by filtration using a 50-nm syringe filter. **a** Internal viral proteins in the culture supernatant were detected by enzyme-linked immunosorbent assay (ELISA). **b** The viral titer was measured as $TCID_{50}$/ml. **c** The *M* gene was detected by qRT–PCR, and **d** the M1 and NP proteins were detected by western blotting. **e** The supernatants of MDCK cells treated with phosphate-buffered saline (PBS) or the PR8 virus (10^1–10^3 $TCID_{50}$/ml) were obtained. After filtration through a 50-nm filter, the nucleoprotein (NP) levels were measured by ELISA. **f** Mice ($n = 4$) were infected with the PR8 virus (32 PFU), and then on Days 0, 1, 3, 5, 7, and 9, NP in the bronchoalveolar lavage fluid (BALF) was detected by ELISA. The data in **a**–**c** are presented as the mean ± standard deviation (SD) from triplicate culture wells. The data in **d** are presented as the mean ± standard error of the mean (SEM). ***$p < 0.001$

Extracellular NP interacts with TLR2 and TLR4 to induce proinflammatory cytokine secretion

Influenza virus infection leads to the recruitment of various immune cells, such as neutrophils, monocytes, dendritic cells (DCs), and T cells, into the lungs [12]. Given that influenza virus proteins exist outside cells, we hypothesized that viral proteins can directly interact with infiltrated immune cells in the lungs. First, we confirmed the infiltration of various immune cells upon viral infection (Supplementary Fig. 2a). NP is one of the most abundant molecules in the influenza virion [13], and it has a highly conserved amino acid sequence observed in various influenza A viruses, including the seasonal influenza virus that infects humans [14]. Therefore, to investigate the effect of NP on the behavior of innate immune cells, we purified recombinant NP (rNP) from the expiCHO cell line at an endotoxin-free level (0.16 EU/mg; Supplementary Fig. 3a–d). We investigated the inflammatory pathway induced by NP in bone marrow-derived macrophages (BMDMs) because macrophages are commonly used in the study of inflammation. When BMDMs were treated with rNP, the mitogen-activated protein (MAP) kinase family and nuclear factor kappa light chain enhancer of activated B cells (NF-κB) were activated from an early time point (15 min) in a dose-dependent manner (Fig. 2a, b). rNP induced the production of proinflammatory cytokines and chemokines, including IL-1ß and IL-6, in BMDMs (Fig. 2c).

Such responses are well-known downstream events of TLR signaling in inflammatory monocytes or macrophages [15]. Therefore, we used TLR-expressing cell lines to evaluate whether rNP can stimulate TLRs. When TLR-expressing reporter cell lines were treated with rNP, the TLR2- and TLR4-expressing cell lines were activated in a dose-dependent manner (Fig. 2d). To investigate the physical interactions between rNP and these two TLRs, BMDMs were treated with rNP, and the cell lysates were immunoprecipitated using anti-TLR2, anti-TLR4, or anti-NP antibodies. In each case, NP, TLR2, and TLR4 were detected in the precipitate, indicating that rNP directly interacted with TLR2 and TLR4 (Fig. 2e). rNP also bound to recombinant TLR2 and TLR4 proteins (Fig. 2f), confirming these interactions. Subsequently, the activation of TLR downstream molecules and the production of proinflammatory factors, except IL-1ß, were significantly reduced in TLR2 KO, TLR4 KO, and TLR2/4 double knockout BMDMs upon NP treatment in a dose-dependent manner, confirming that the immunostimulatory effect of rNP depends upon TLR2 and TLR4 (Fig. 2g and Supplementary Fig. 4a–c).

NP exists in the form of trimers or larger oligomers in equilibrium with monomers [16, 17]. rNP was divided into fractions of less and greater than 100 kDa to assess which quaternary structure of NP predominates in TLR stimulation. We observed that TLR4 stimulation was significantly increased when rNP with a molecular weight of 100 kDa or greater was used (Fig. 2h), suggesting that oligomeric NP has a greater stimulatory effect than monomeric NP. To confirm this possibility, we prepared R416A-mutant NP, which does not form oligomers [16], and we observed that R416A-mutant NP could not stimulate TLR4 (Fig. 2i). Purified recombinant NP is known to form trimers after 30–60 min at room temperature [16, 17]. Therefore, we purified and incubated rNP at various temperatures to assess the TLR-stimulating activity and observed that incubation with rNP at 25 °C for 18 h showed the highest TLR-stimulating activity (Fig. 2j). These findings suggest that extracellular NP can stimulate TLR4 by forming a quaternary structure of oligomers rather than monomers.

Extracellular NP activates the NLRP3 inflammasome

Activation of NF-κB increases the levels of pro-IL-1ß, but the production of active IL-1ß requires the activation of the inflammasome [18]. Based on the detection of active IL-1ß following rNP treatment in BMDMs (Fig. 2c), we sought to evaluate NLRP3 inflammasome activation by exogenous NP. When BMDMs were treated with rNP, they produced IL-1ß in an rNP

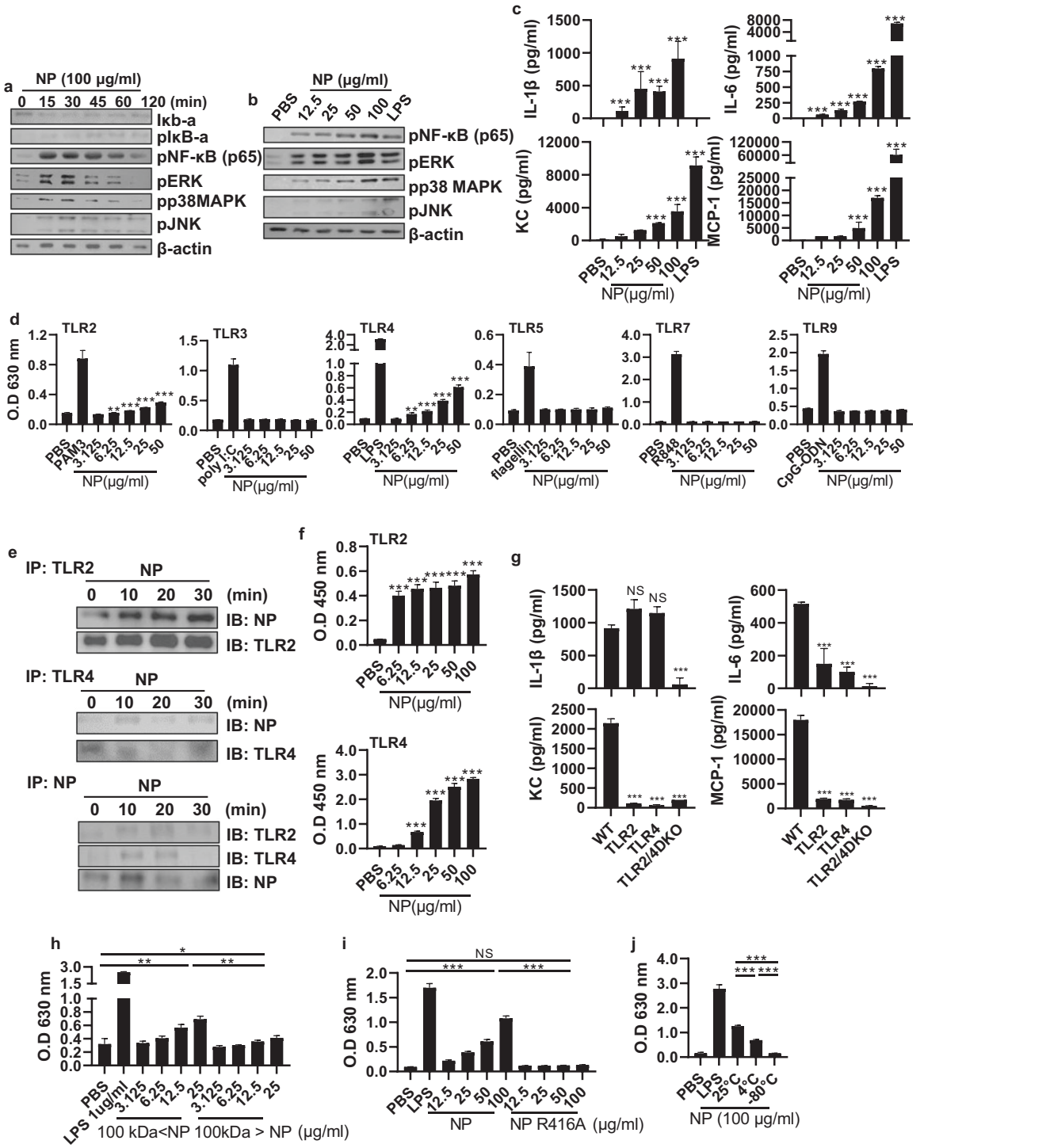

Fig. 2 Oligomeric NP interacts with and activates TLR2 and TLR4 a Bone marrow-derived macrophages (BMDMs) were treated with recombinant NP (rNP; 100 μg/ml) for 0–120 min or **b** with rNP (12.5–100 μg/ml) for 30 min. After the incubation period, the activation of the NF-κB and MAPK pathways was detected by western blotting. **c** BMDMs were treated with rNP (12.5–100 μg/ml) for 20 h, and the levels of cytokines and chemokines in the cell culture supernatant were measured by ELISA. **d** HEK293 cells expressing TLR2, TLR3, TLR4, TLR5, TLR7, or TLR9 were incubated with PBS, rNP (12.5–100 μg/ml), or the corresponding ligands (1 μg/ml PAM3, 1 μg/ml poly I:C, 100 ng/ml LPS, 1 μg/ml flagellin, 1 μg/ml R848, or 1 μg/ml CpG oligodeoxynucleotide) for 20 h. After the incubation period, the absorbance was recorded at 630 nm. **e** BMDMs were treated with rNP (0–30 min), followed by immunoprecipitation (IP) with anti-Toll-like receptor (TLR) 2, anti-TLR4, and anti-NP antibodies. TLR2, TLR4, and NP in the coprecipitate were detected by western blotting. **f** rNP (6.25–100 μg/ml) was added to each well coated with recombinant TLR (rTLR) 2 (2 μg/ml) and rTLR4 (2 μg/ml). After sequential incubation and washing, NP bound to rTLRs was detected by ELISA. **g** TLR2 KO, TLR4 KO, and TLR2/4 DKO BMDMs were treated with rNP (100 μg/ml) for 20 h. After the incubation period, the cytokine and chemokine levels in the cell culture supernatant were determined by ELISA. HEK293 cells expressing TLR4 were cultured with PBS, LPS, **h** 100-kDa size-fractionated rNP (3.125–25 μg/ml), **i** the rNP R416A mutant (12.5–100 μg/ml), **j** or 25 °C, 4 °C, and −80 °C-incubated rNP (12.5–100 μg/ml). After 20 h, the absorbance was recorded at 630 nm. Data are presented as the mean ± SD from triplicate culture wells. ***$p < 0.001$, **$p < 0.01$, *$p < 0.05$

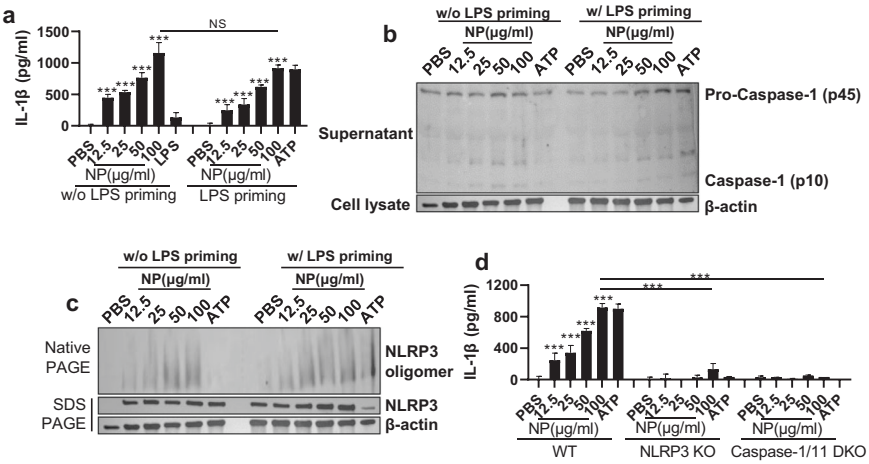

Fig. 3 NP induces activation of the NLRP3 inflammasome BMDMs were pretreated with LPS (100 ng/ml) for 3 h and then treated with NP (12.5–100 μg/ml) or ATP for 20 h. **a** The levels of IL-1β in the cell culture supernatant were detected by ELISA. **b** Caspase-1 activation in the cell culture supernatant was detected by western blotting. **c** NLRP3 oligomerization in the cell lysate was detected by native-PAGE western blotting. **d** NLRP3 KO and caspase-1/11 KO BMDMs were subjected to LPS priming 3 h before rNP (12.5–100 μg/ml) or ATP exposure; after 20 h, IL-1β in the cell culture supernatant was detected by ELISA. Data are presented as the mean ± SD from triplicate culture wells. ***$p < 0.001$, **$p < 0.01$, *$p < 0.05$

dose-dependent manner (Fig. 3a). rNP also triggered the activation of caspase-1 and oligomerization of NLRP3 (Fig. 3b, c). Notably, all of these responses were independent of lipopolysaccharide (LPS) priming, which indicates that NP is able to activate both TLR-dependent NK-κB pathways and NLRP3-dependent inflammasome pathways. Consistent with our observations, extracellular NP-triggered IL-1ß production was abolished in NLRP3 KO and caspase-1/11 double KO BMDMs (Fig. 3d), confirming that the induction of IL-1ß is NLRP3 inflammasome dependent.

Extracellular NP induces proinflammatory cytokines through activation of TLR4 and the NLRP3 inflammasome in human cell lines We next investigated whether influenza virus infection induces internal viral protein release and TLR and NLRP3 inflammasome activation and whether extracellular NP can be applied to human cells. PR8 virus-infected THP-1 and A549 cells showed induction of internal viral proteins, including NP release, similar to that observed in the MDCK cell line (Supplementary Fig. 5a–c). In addition, rNP induced the activation of the TLR signaling cascade and the production of IL-1ß and IL-6 in THP-1 and A549 cells, which represent human monocytes and lung epithelial cells, respectively (Supplementary Fig. 5d–g). Furthermore, a TLR4 inhibitor decreased IL-6 production, and an NLRP3 inhibitor reduced IL-1ß production in NP-treated THP-1 cells (Supplementary Fig. 5h, i). These results indicate that the release of viral proteins upon viral infection and the function of extracellular NP are not limited to the mouse model studied.

Extracellular NP increases the infectivity of influenza virus by upregulating trypsin

Proteolytic cleavage of HA precursor (HA0) into the HA1 and HA2 subunits is a critical event for membrane fusion and productive infection by influenza virus [19]. During this process, trypsin derived from host cells plays an indispensable role [20], and viral infection upregulates the expression of trypsin via proinflammatory cytokines such as IL-1ß and IL-6 (Supplementary Fig. 6a) [21, 22]. This series of reactions is known as the 'influenza virus-cytokine-trypsin cycle'. As we observed increases in these cytokines induced by NP stimulation (Figs. 2c and 3a, and Supplementary Fig. 4c), we next assessed whether NP upregulates trypsin in host cells. When BMDMs were treated with rNP, trypsin was significantly upregulated in a dose-dependent manner (Fig. 4a). Consistent with this, the effect of rNP was TLR2 and TLR4 dependent, while the level of trypsin following rNP treatment was significantly decreased in TLR2-deficient, TLR4-deficient, TLR2/4 double-deficient and downstream adaptor molecule (MyD88 and TRIF)-deficient BMDMs (Fig. 4b, c). Trypsin expression was also decreased in NLRP3- and caspase-1/11-deficient BMDMs (Fig. 4d). Finally, we evaluated whether NP-triggered trypsin cleaves HA0 into an active form and increases viral infectivity. When the virus was incubated in conditioned medium from rNP-treated BMDMs, cleaved HA subunits were detected (Fig. 4e). In addition, when MDCK cells were infected with the incubated virus, viral replication was significantly increased (Fig. 4f). To investigate whether trypsin upregulation induced by extracellular NP treatment increases viral replication, rNP-treated BMDM supernatants were incubated with the virus and a protease inhibitor for 1 h. Subsequently, upon infection with the incubated virus, viral replication was significantly reduced in the protease inhibitor-treated group (Fig. 4g). These data show that extracellular NP induces trypsin in host cells, thereby increasing viral infectivity by enhancing the proteolytic cleavage of HA.

Extracellular NP contributes to an increased viral titer and influenza pathogenicity in vivo

Given that NP increases viral infectivity through the 'influenza virus-cytokine-trypsin cycle' in vitro, we next investigated whether NP affects the host immune response and influenza pathogenicity in vivo. When mice were cotreated with influenza virus and trypsin or pretreated with IL-1ß and IL-6 and then infected with influenza virus, increased weight loss and a decreased survival rate were observed, suggesting that the influenza virus-cytokine-trypsin cycle also plays an important role in vivo (Supplementary Fig. 6b–e). When mice were intranasally treated with rNP, the levels of IL-1ß, IL-6, and trypsin were significantly increased in the BALF at 6 h (Fig. 5a). Nonetheless, NP-induced inflammatory cytokines per se did not have significant effects on lung epithelial cell integrity or lung lesions (Fig. 5b, c).

To identify which cell population mainly interacts with NP, we isolated immune cells from lung tissue and incubated them with Alexa488-labeled rNP. The major populations of Alexa488-positive cells were neutrophils, monocytes, and macrophages (Fig. 5d), indicating that these immune cells, which express TLR2 and TLR4 [23], were the primary cells interacting with NP.

We next evaluated whether rNP increases viral replication and influenza pathogenicity in vivo. Mice were treated with rNP intranasally and, 3 days later, infected with a sublethal dose of

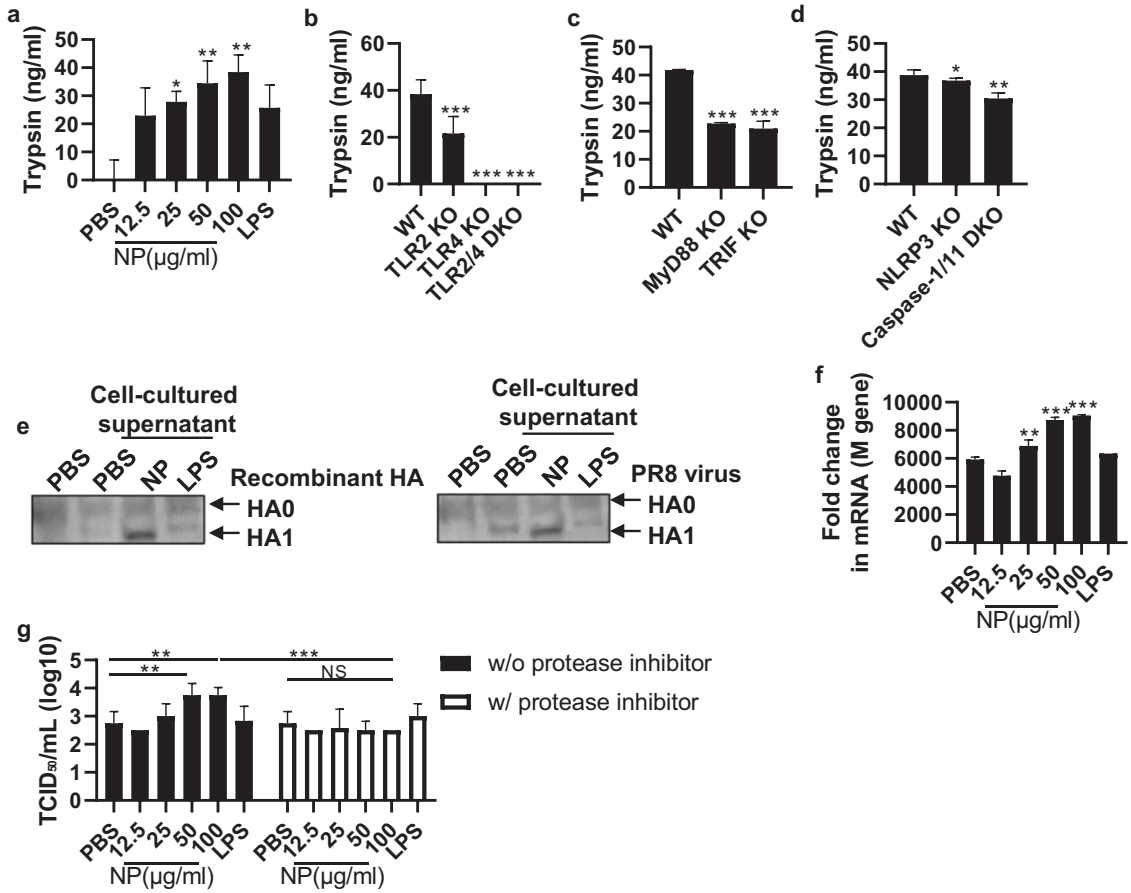

Fig. 4 NP increases influenza virus infectivity via trypsin upregulation a BMDMs were treated with rNP (12.5–100 μg/ml) or LPS (1 μg/ml) for 20 h. Then, the level of trypsin in the cell culture supernatant was measured by ELISA. BMDMs derived from each KO mouse strain were treated with rNP (100 μg/ml) for 20 h. **b** The trypsin levels in TLR2 KO, TLR4 KO, and TLR2/4 DKO BMDMs. **c** The trypsin levels in MyD88 KO and TRIF KO BMDMs. **d** The trypsin levels of NLRP3 KO and caspase-1/11 KO BMDMs in the cell culture supernatant were detected by ELISA. **e** Recombinant hemagglutinin (HA) protein or influenza virus was incubated with rNP-treated BMDM culture supernatant for 1 h. Then, hemagglutinin cleavage was detected by western blotting. **f** BMDMs were treated with rNP (12.5–100 μg/ml), and the culture supernatant was collected and used to treat the PR8 virus (10^3 $TCID_{50}$/ml) for 1 h. Then, MDCK cells were infected with the treated virus. After a 72-h incubation, the *M* gene levels in the infected cells were measured by qRT–PCR. **g** rNP (12.5–100 μg/ml)-treated BMDM culture supernatants were incubated with the PR8 virus with (or without) a protease inhibitor for 1 h, and then, MDCK cells were infected with the incubated virus. After 72 h of infection, the viral titer was detected as $TCID_{50}$/ml. Data are presented as the mean ± SD from triplicate culture wells. ***$p < 0.001$, **$p < 0.01$, *$p < 0.05$

influenza virus. Pretreatment with rNP significantly and dose-dependently decreased the survival rate upon subsequent infection with influenza virus compared to PBS pretreatment (Fig. 5e). Consistently, the viral titer in the lungs increased with increasing rNP doses (Fig. 5f). In addition, the albumin levels in the BALF were increased 5 days after infection with rNP pretreatment, and histological findings also showed that rNP pretreatment increased viral pathogenicity (Fig. 5g, h). In addition, treatment with rNP at 3 days post-viral infection increased the mouse fatality rate (Fig. 5i). However, in TLR4 KO and NLRP3 KO mice, pretreatment with rNP did not increase the fatality rate (Supplementary Fig. 7c, d). Altogether, these data indicate that extracellular NP substantially influences the viral titer and pathogenicity of influenza virus, mainly via stimulation of TLR4 and NLRP3 inflammasome pathways in vivo.

Anti-NP antibody reduces the viral titer and ameliorates influenza pathogenicity in vivo

Given that NP released from infected cells increases influenza pathogenesis by triggering IL-1β and IL-6 and then trypsin, we next investigated whether NP blockade decreases the levels of these soluble factors and reduces viral replication and influenza pathogenicity in vivo. We first assessed the inhibitory effect of anti-NP antibodies on viral infection and the interaction between NP and TLR4 in vitro. Although anti-NP serum isolated from NP-immunized mice was not able to neutralize influenza virus in vitro (Supplementary Fig. 8a), it significantly reduced the binding of rNP to recombinant TLR4 (Fig. 6a). Moreover, BMDMs were treated with filtered PR8 virus-infected cell culture supernatant containing anti-NP serum. Anti-NP serum reduced proinflammatory cytokine production induced by the filtered supernatant, while naïve serum did not produce this effect (Fig. 6b, c).

To investigate whether anti-NP serum reduces viral pathogenicity by dampening the influenza virus-cytokine-trypsin cycle in vivo, influenza virus-infected mice were treated with anti-NP serum, and body weight loss and the BALF viral titer were significantly reduced (Fig. 6d, e, and Supplementary Fig. 8b). Weight loss and the fatality rate were also significantly decreased by injecting IgG purified from immune poly serum in a dose-dependent manner (Supplementary Fig. 8c). On Day 5 post-infection with anti-NP serum, the albumin level in the BALF was significantly decreased compared to that in the naïve serum-treated group, and anti-NP serum treatment also reduced pathogenicity, as indicated by histological findings (Fig. 6f, g). To further investigate the mechanism by which NP blockade

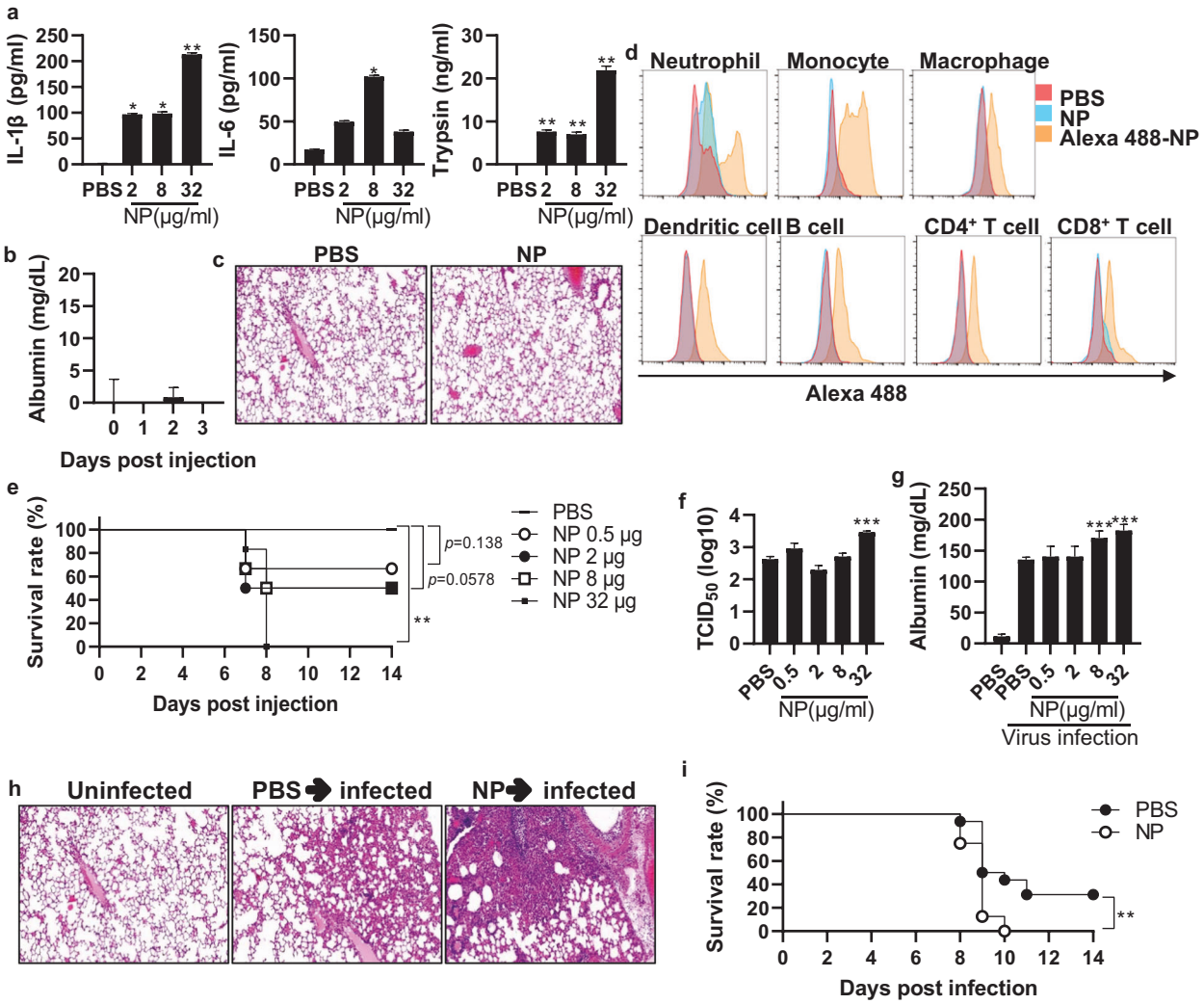

Fig. 5 NP contributes to an increased viral titer and influenza pathogenicity in vivo a Mice (n = 5) were treated intranasally with rNP (2–32 μg/mouse). After 6 h, the levels of IL-1β, IL-6, and trypsin in the BALF were measured by ELISA. **b** Mice (n = 5) were treated intranasally with rNP (32 μg/mouse), and albumin was measured in the BALF daily for three days. **c** Mice were treated intranasally with rNP (32 μg/mouse), and the histology of lung tissue was assessed after hematoxylin-eosin (H&E) staining. **d** Isolated total lung cells were incubated with Alexa 488-labeled rNP (100 μg/ml) for 15 min, and NP-bound cells were evaluated by flow cytometry. **e** Mice ($n = 6$) were treated intranasally with NP (2–32 μg/ml) and subsequently infected with the PR8 virus (32 PFU) on Day 3. The survival rate was monitored for two weeks. **f**–**h** At five days post-infection, the viral load and the level of albumin in the BALF were determined. Histological analysis of lung tissue was performed after H&E staining. **i** Mice ($n = 16$) were treated intranasally with NP (2–32 μg/ml) three days prior to PR8 viral infection (32 PFU). Upon infection, the survival rate was monitored for two weeks. Data are presented as the mean ± SEM. ***$p < 0.001$, **$p < 0.01$, *$p < 0.05$

alleviates influenza severity in vivo, we measured the levels of various soluble factors following viral infection and anti-NP serum treatment. The levels of IL-1ß, IL-6, and trypsin were significantly decreased in mice in the anti-NP serum-treated group on Day 5 (Fig. 6h).

Anti-NP antibodies, which cannot neutralize influenza virus, have been shown to have anti-influenza effects in vivo, presumably via antibody-dependent cellular cytotoxicity (ADCC) [24]. To verify whether the anti-influenza effect of anti-NP serum is mediated by ADCC, we investigated the effect of anti-NP serum on influenza after depletion of NK cells. Intraperitoneally injecting 100 μg of anti-NK1.1 antibody on Day 2 depleted approximately 95% of NK cells in vivo (Supplementary Fig. 9a). Even after the depletion of NK cells, the survival rate of mice in the anti-NP serum-injected group was significantly increased compared to that of mice in the naïve serum-injected group (Supplementary Fig. 9b). This indicates that anti-NP antibodies can lower, at least partially, influenza pathogenicity in an ADCC-independent manner.

Altogether, these results indicate that anti-NP serum or purified antibodies can inhibit the interaction between NP and TLR4, thereby leading to a decrease in the production of proinflammatory cytokines and trypsin and eventually a decrease in pathogenicity in vivo.

DISCUSSION

Influenza virus is one of the major causes of infectious disease worldwide, and its pathogenic mechanism has been widely studied. The interaction between the virus and host innate immunity is thought to be essential for type I IFN-mediated antiviral defense and the induction of antigen-specific immune responses [25] but is often highly associated with viral pathogenicity [26]. In this study, we suggest a novel mechanism by which viral NP released from influenza virus-infected cells interacts with host cell PRRs to increase influenza pathogenicity. In particular, extracellular NP stimulates TLRs on the cell surface,

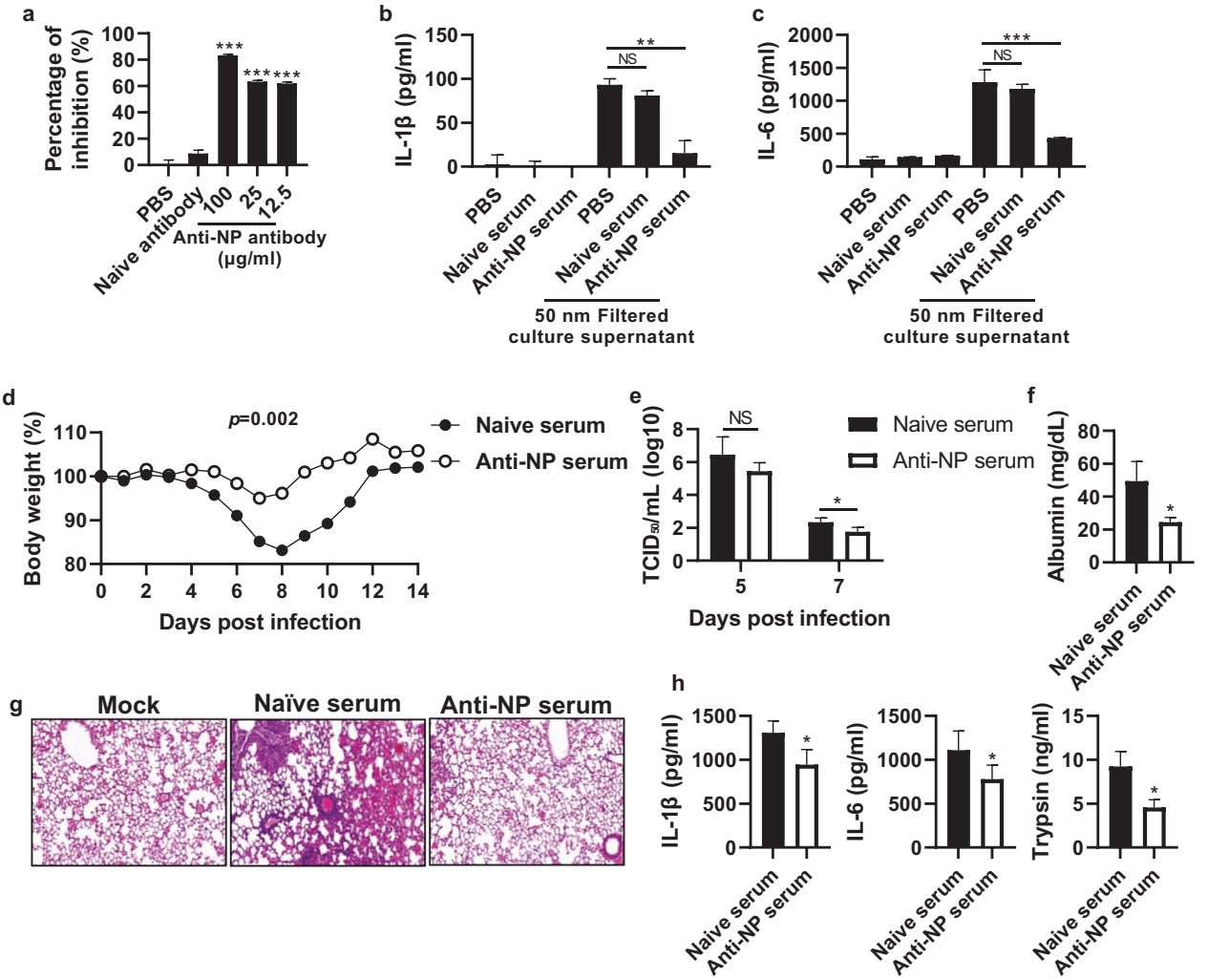

Fig. 6 Anti-NP antibody inhibits the NP-TLR4 interaction and reduces influenza virus pathogenicity a An anti-NP antibody was incubated with rNP for 1 h at 25 °C, and then the antibody-treated NP was added to an ELISA plate coated with rTLR4 (2 μg/ml). After sequential incubation and washing, NP bound to rTLR4 was detected by ELISA. **b**, **c** MDCK cells were infected with the PR8 virus (10^3 $TCID_{50}$/ml) for 72 h, and the cell culture supernatant was filtered using a 50-nm syringe filter. The filtered supernatant was incubated with naïve serum (1:100 diluted) or anti-NP serum (1:100 diluted). Subsequently, BMDMs were treated with the filtered supernatant for 20 h, and the levels of cytokines and chemokines in the cell culture supernatants were measured by ELISA. Mice ($n = 6$) were infected with the PR8 virus (32 PFU) and then injected with anti-NP serum (200 μl/mouse) intraperitoneally daily for three days. **d** Body weight was monitored for two weeks. **e** The $TCID_{50}$ was evaluated using BALF samples obtained on Days 5 and 7 post-infection. **f**, **g** The albumin level in the BALF was measured, and the histology of lung tissue was assessed by H&E staining at 5 days post-infection. **h** Proinflammatory cytokines and trypsin in the BALF were measured by ELISA at five days post-infection. The data in **a** are presented as the mean ± SD from triplicate culture wells. The data in **b**–**f** are presented as the mean ± SEM. ***$p < 0.001$, **$p < 0.01$, *$p < 0.05$

suggesting that internal viral proteins may have different functions at different locations.

Interactions between influenza virus proteins and host cell proteins affect the adaptive immune response, viral proliferation, and/or disease pathology. NP binds to ZBP-1 and activates the NLRP3 inflammasome to induce lung epithelial cell death [27], and M2 binds to the autophagy regulatory protein LC3 to inhibit autophagy and increase viral stability [28]. Furthermore, NS1 inhibits the type I IFN response through direct binding with RIG-1 and MAVS [29]. To date, these functions have been studied in the cytoplasm of infected cells. However, in this study, we demonstrated that influenza virus proteins, which are considered to exist only in the cytoplasm or inside the virion, can also have effects outside of host cells. NP was present in cell-free and virion-free forms outside infected cells and directly bound to TLR2 and TLR4 to induce innate immune responses. We also observed that various other influenza virus proteins, such as M1 and PA, existed outside infected cells. Therefore, the extracellular functions of other internal viral proteins need to be further investigated.

It has been generally regarded that internal influenza virus proteins such as NP and matrix 1 (M1) function inside infected cells, whereas external proteins such as hemagglutinin (HA) and neuraminidase (NA) function outside cells [30]. In this study, however, we showed that internal viral proteins exist outside of cells and play an immunoregulatory role in the extracellular space. Although we did not show the exact mechanism by which NP is secreted or released from infected cells, there are several possible mechanisms: (1) Influenza virus induces lytic cell death, resulting in the release of cellular viral proteins into the extracellular space [31]. (2) During the replication of influenza virus, M1 interacts with both phosphatidylserine in the plasma membrane on its apical side [32] and the ribonucleoprotein (RNP) complex on its basal side [33]. As infected cells undergo apoptosis, PS in the inner

leaflet flips to the outer leaflet of the plasma membrane, and hence, the phosphatidylserine-associated M1 and NP in the RNP complex can be exposed to the extracellular space [34]. (3) NP might be secreted or released from infected cells in the form of a complex with the high-mobility-group box 1 protein [35, 36]. Further study is required to identify the underlying mechanism for the release of internal viral proteins.

TLR2 and TLR4 exist in the cytoplasmic membrane and are known to recognize PAMPs that are mainly derived from bacteria [37]. In our study, we identified for the first time the direct interactions between influenza virus NP and TLR2 or TLR4. The interactions of different viral proteins and TLRs have been previously reported. Some of these proteins include the fusion (F) protein of respiratory syncytial virus, glycoprotein of Ebola virus, and glycoprotein of vesicular stomatitis virus [6, 8, 38]. Recently, the spike protein of SARS-CoV-2 was also reported to activate TLR2 and trigger an inflammatory reaction [9]. However, these proteins are present outside of the virion and therefore can interact through simple physical proximity between the virus and immune cells. Here, we demonstrated that NP, which is present inside the virion, activates TLR2 and TLR4 through translocation and that this mechanism can increase viral infectivity and pathogenicity.

HA proteolytic cleavage is an important step in influenza viral infectivity. In this process, serine proteases, such as trypsin, play an important role. Studies have shown that viral infection increases under conditions of high trypsin secretion and that treatment with trypsin inhibitors inhibits influenza virus [39]. Viral proteolytic cleavage by serine proteases is well known for herpesvirus glycoprotein B, coronavirus spike protein, dengue virus envelope proteins, and influenza virus HA, and this process is essential for viral infection [40–42]. In our study, NP did not directly induce lung inflammation or abnormal symptoms; however, it induced cytokines, including IL-1ß and IL-6, and increased trypsin expression. Moreover, NP-induced trypsin increased HA protein cleavage in vitro and viral infection both in vitro and in vivo. This is a new positive feedback mechanism by which viral proteins increase HA proteolytic cleavage through the cytokine–trypsin cycle to increase viral infectivity.

Here, influenza virus NP was shown to directly bound to TLR2 and TLR4 and stimulate effective downstream signaling. As mentioned above, studies have shown that several viral surface proteins stimulate TLRs to increase pathogenicity [6, 8, 9, 43]; however, studies have not reported that the nucleocapsid or capsid proteins perform such functions. Studies have shown that treatment of cells with viral nuclear proteins in vitro stimulates innate immune activities, such as cytokine secretion. When the SARS-CoV nucleocapsid protein was administered to the mouse nasal cavity, TNF-α and IFN-γ were found to be increased in the lungs [44]. Furthermore, the highly positively charged hepatitis B virus core antigen protein induced the secretion of cytokines, such as TNF-α and IL-6, in human macrophage cell lines through an interaction with heparan sulfate [45]. In our study, we observed that NP multimers induced TLR4 activation, suggesting that the quaternary structure of NP plays an essential role in the NP-TLR4 interaction. The quaternary ring structure of influenza virus NP is similar to that of VSV and molluscum contagiosum virus NPs [46], and the structure of VSV is similar to that of various negative-strand RNA viruses, including paramyxoviridea [47, 48]. Additional structure-based studies are required to create a better understanding of the interactions between the common structures of viral nucleo- or nucleocapsid proteins and TLRs.

In the present study, plasma or purified IgG fractions against NP inhibited NP-TLR4 binding in vitro and reduced inflammatory cytokine and trypsin levels and pathogenicity in vivo. Previous studies have demonstrated the in vivo antiviral effects of anti-NP antibodies [49, 50]. Anti-NP antibodies do not directly neutralize influenza virus; however, the data have been interpreted to indicate that these antibodies inhibit influenza virus through NK cell-dependent ADCC [24]. However, this mechanism has only been demonstrated in vitro, and the antiviral mechanism of anti-NP antibodies mediated through NK cells in vivo has not been reported. In our study, we found that anti-NP serum increased the survival rate of infected mice, including even NK cell-depleted mice, compared to control serum. This finding suggests that the antiviral effects of anti-NP antibodies may not be fully dependent on NK cells. Furthermore, studies have reported that anti-NP antibody treatment in FcR-deficient mice can provide protection against influenza virus infection [50]. These results suggest that anti-NP can inhibit influenza virus infection through mechanisms other than NK cell-dependent ADCC.

In conclusion, we demonstrate a novel pathogenic role for NP in the pathogenesis of influenza virus. NP, which has been considered to exist inside infected cells or virions, is translocated to the extracellular compartment and then activates neighboring immune cells via TLR4 and NLRP3. Considering that many viruses causing acute respiratory infection induce lytic cell death, this finding highlights the potential pathogenic role of internal viral proteins mediated via interactions with PRRs present on uninfected neighboring immune cells.

REFERENCES

1. Couch RB. Seasonal inactivated influenza virus vaccines. Vaccine. 2008;26:D5–9.
2. Takeuchi O, Akira S. Pattern recognition receptors and inflammation. Cell. 2010;140:805–20.
3. Chen X, Liu S, Goraya MU, Maarouf M, Huang S, et al. Host immune response to influenza a virus infection. Front Immunol. 2018;9:320.
4. McAuley JL, Tate MD, MacKenzie-Kludas CJ, Pinar A, Zeng W, et al. Activation of the NLRP3 inflammasome by IAV virulence protein PB1-F2 contributes to severe pathophysiology and disease. PLoS Pathog. 2013;9:e1003392.
5. Ichinohe T, Pang IK, Iwasaki A. Influenza virus activates inflammasomes via its intracellular M2 ion channel. Nat Immunol. 2010;11:404–10.
6. Okumura A, Pitha PM, Yoshimura A, Harty RN. Interaction between Ebola virus glycoprotein and host toll-like receptor 4 leads to induction of proinflammatory cytokines and SOCS1. J Virol. 2010;84:27–33.
7. Uno N, Ross TM. Dengue virus and the host innate immune response. Emerg Microbes Infect. 2018;7:167.
8. Georgel P, Jiang Z, Kunz S, Janssen E, Mols J, et al. Vesicular stomatitis virus glycoprotein G activates a specific antiviral Toll-like receptor 4-dependent pathway. Virology. 2007;362:304–13.
9. Zheng M, Karki R, Williams EP, Yang D, Fitzpatrick E, et al. TLR2 senses the SARS-CoV-2 envelope protein to produce inflammatory cytokines. Nat Immunol. 2021;22:829–38.
10. Ha SJ, Jeon BY, Kim SC, Kim DJ, Song MK, et al. Therapeutic effect of DNA vaccines combined with chemotherapy in a latent infection model after aerosol infection of mice with Mycobacterium tuberculosis. Gene Ther. 2003;10:1592–9.
11. Arias CF, Escalera-Zamudio M, Soto-Del Rio Mde L, Cobian-Guemes AG, Isa P, et al. Molecular anatomy of 2009 influenza virus A (H1N1). Arch Med Res. 2009;40:643–54.
12. Lamichhane PP, Samarasinghe AE. The Role of Innate Leukocytes during Influenza Virus Infection. J Immunol Res. 2019;2019:8028725.
13. Kummer S, Flottmann M, Schwanhausser B, Sieben C, Veit M, et al. Alteration of protein levels during influenza virus H1N1 infection in host cells: a proteomic survey of host and virus reveals differential dynamics. PLoS One. 2014;9:e94257.
14. Kukol A, Hughes DJ. Large-scale analysis of influenza A virus nucleoprotein sequence conservation reveals potential drug-target sites. Virology. 2014;454-5:40–47.
15. K Ozato, H Tsujimura and T Tamura, Toll-like receptor signaling and regulation of cytokine gene expression in the immune system. Biotechniques, 2002. 70, 72 passim.
16. Chenavas S, Estrozi LF, Slama-Schwok A, Delmas B, Di Primo C, et al. Monomeric nucleoprotein of influenza A virus. PLoS Pathog. 2013;9:e1003275.
17. Ng AK, Zhang H, Tan K, Li Z, Liu JH, et al. Structure of the influenza virus A H5N1 nucleoprotein: implications for RNA binding, oligomerization, and vaccine design. FASEB J. 2008;22:3638–47.
18. Yang Y, Wang H, Kouadir M, Song H, Shi F. Recent advances in the mechanisms of NLRP3 inflammasome activation and its inhibitors. Cell Death Dis. 2019;10:128.
19. Bertram S, Glowacka I, Steffen I, Kuhl A, Pohlmann S. Novel insights into proteolytic cleavage of influenza virus hemagglutinin. Rev Med Virol. 2010;20:298–310.

20. Kido H. Influenza virus pathogenicity regulated by host cellular proteases, cytokines and metabolites, and its therapeutic options. Proc Jpn Acad Ser B Phys Biol Sci. 2015;91:351–68.
21. Indalao IL, Sawabuchi T, Takahashi E, Kido H. IL-1beta is a key cytokine that induces trypsin upregulation in the influenza virus-cytokine-trypsin cycle. Arch Virol. 2017;162:201–11.
22. Kido H, Takahashi E, Kimoto T. Role of host trypsin-type serine proteases and influenza virus-cytokine-trypsin cycle in influenza viral pathogenesis. Pathogenesis-based therapeutic options. Biochimie. 2019;166:203–13.
23. Janssens S, Beyaert R. Role of Toll-like receptors in pathogen recognition. Clin Microbiol Rev. 2003;16:637–46.
24. Vanderven HA, Ana-Sosa-Batiz F, Jegaskanda S, Rockman S, Laurie K, et al. What lies beneath: antibody dependent natural killer cell activation by antibodies to internal influenza virus proteins. EBioMedicine. 2016;8:277–90.
25. McNab F, Mayer-Barber K, Sher A, Wack A, O'Garra A. Type I interferons in infectious disease. Nat Rev Immunol. 2015;15:87–103.
26. Davidson S, Crotta S, McCabe TM, Wack A. Pathogenic potential of interferon alphabeta in acute influenza infection. Nat Commun. 2014;5:3864.
27. Kuriakose T, Man SM, Malireddi RK, Karki R, Kesavardhana S, et al. ZBP1/DAI is an innate sensor of influenza virus triggering the NLRP3 inflammasome and programmed cell death pathways. Sci Immunol., 2016;1:aag2045.
28. Beale R, Wise H, Stuart A, Ravenhill BJ, Digard P, et al. A LC3-interacting motif in the influenza A virus M2 protein is required to subvert autophagy and maintain virion stability. Cell Host Microbe. 2014;15:239–47.
29. Jureka AS, Kleinpeter AB, Tipper JL, Harrod KS, Petit CM. The influenza NS1 protein modulates RIG-I activation via a strain-specific direct interaction with the second CARD of RIG-I. J Biol Chem. 2020;295:1153–64.
30. Patterson S, Oxford JS. Analysis of antigenic determinants on internal and external proteins of influenza virus and identification of antigenic subpopulations of virions in recent field isolates using monoclonal antibodies and immunogold labelling. Arch Virol. 1986;88:189–202.
31. Balachandran S, Rall GF. Benefits and Perils of Necroptosis in Influenza Virus Infection. J Virol., 2020;94:e01101-19.
32. Hofer CT, Di Lella S, Dahmani I, Jungnick N, Bordag N, et al. Structural determinants of the interaction between influenza A virus matrix protein M1 and lipid membranes. Biochim Biophys Acta Biomembr. 2019;1861:1123–34.
33. Ye Z, Liu T, Offringa DP, McInnis J, Levandowski RA. Association of influenza virus matrix protein with ribonucleoproteins. J Virol. 1999;73:7467–73.
34. Marino G, Kroemer G. Mechanisms of apoptotic phosphatidylserine exposure. Cell Res. 2013;23:1247–8.
35. Moisy D, Avilov SV, Jacob Y, Laoide BM, Ge X, et al. HMGB1 protein binds to influenza virus nucleoprotein and promotes viral replication. J Virol. 2012;86:9122–33.
36. Murao A, Aziz M, Wang H, Brenner M, Wang P. Release mechanisms of major DAMPs. Apoptosis. 2021;26:152–62.
37. O'Neill LA, Golenbock D, Bowie AG. The history of Toll-like receptors - redefining innate immunity. Nat Rev Immunol. 2013;13:453–60.
38. Kurt-Jones EA, Popova L, Kwinn L, Haynes LM, Jones LP, et al. Pattern recognition receptors TLR4 and CD14 mediate response to respiratory syncytial virus. Nat Immunol. 2000;1:398–401.
39. Laporte M, Naesens L. Airway proteases: an emerging drug target for influenza and other respiratory virus infections. Curr Opin Virol. 2017;24:16–24.
40. Bertram S, Glowacka I, Muller MA, Lavender H, Gnirss K, et al. Cleavage and activation of the severe acute respiratory syndrome coronavirus spike protein by human airway trypsin-like protease. J Virol. 2011;85:13363–72.
41. Biedrzycka A, Cauchi MR, Bartholomeusz A, Gorman JJ, Wright PJ. Characterization of protease cleavage sites involved in the formation of the envelope glycoprotein and three non-structural proteins of dengue virus type 2, New Guinea C strain. J Gen Virol. 1987;68:1317–26.
42. Okazaki K. Proteolytic cleavage of glycoprotein B is dispensable for in vitro replication, but required for syncytium formation of pseudorabies virus. J Gen Virol. 2007;88:1859–65.
43. P Rallabhandi, RL Phillips, MS Boukhvalova, LM Pletneva, KA Shirey, et al., Respiratory syncytial virus fusion protein-induced toll-like receptor 4 (TLR4) signaling is inhibited by the TLR4 antagonists Rhodobacter sphaeroides lipopolysaccharide and eritoran (E5564) and requires direct interaction with MD-2. mBio, 2012.3.
44. Zhu YG, Qu JM. Differential characteristics of the early stage of lung inflammation induced by SARS-CoV Nucleocapsid protein related to age in the mouse. Inflamm Res. 2009;58:312–20.
45. Cooper A, Tal G, Lider O, Shaul Y. Cytokine induction by the hepatitis B virus capsid in macrophages is facilitated by membrane heparan sulfate and involves TLR2. J Immunol. 2005;175:3165–76.
46. Morin B, Kranzusch PJ, Rahmeh AA, Whelan SP. The polymerase of negative-stranded RNA viruses. Curr Opin Virol. 2013;3:103–10.
47. Luo M, Terrell JR, McManus SA. Nucleocapsid structure of negative strand RNA virus. Viruses. 2020;12:835.
48. Sanchez A, Banerjee AK, Furuichi Y, Richardson MA. Conserved structures among the nucleocapsid proteins of the paramyxoviridae: complete nucleotide sequence of human parainfluenza virus type 3 NP mRNA. Virology. 1986;152:171–80.
49. Carragher DM, Kaminski DA, Moquin A, Hartson L, Randall TD. A novel role for non-neutralizing antibodies against nucleoprotein in facilitating resistance to influenza virus. J Immunol. 2008;181:4168–76.
50. LaMere MW, Lam HT, Moquin A, Haynes L, Lund FE, et al. Contributions of antinucleoprotein IgG to heterosubtypic immunity against influenza virus. J Immunol. 2011;186:4331–9.

ACKNOWLEDGEMENTS

This work was supported by grants from the Bio & Medical Technology Development Program of the National Research Foundation of Korea (NRF) (2018M3A9H4077992) and the KRIBB Initiative program (KGM9942112) funded by the Korean government (Ministry of Science & ICT).

AUTHOR CONTRIBUTIONS

Study conception and design: CUK, DJK. Methodology: CUK, YJJ, JHP. Analysis and interpretation of results: CUK, YJJ, PL, MSL, YSK, DJK. Investigation: CUK, YJJ. Validation: CUK, YSK, DJK. Resources: CUK, YJJ, JHP, DJK. Original draft preparation: CUK. Draft review & editing: CUK, YSK, DJK. Final edition: DJK. Supervision: YSK, DJK. All authors reviewed the results and approved the final version of the manuscript.

FUNDING

This work was supported by grants from the Bio & Medical Technology Development Program of the National Research Foundation of Korea (NRF) (2018M3A9H4077992) and the KRIBB Initiative program (KGM9942112) funded by the Korean government (Ministry of Science & ICT).

COMPETING INTERESTS

The authors declare no competing interests.

ADDITIONAL INFORMATION

Supplementary information The online version contains supplementary material available at https://doi.org/10.1038/s41423-022-00862-5.

Correspondence and requests for materials should be addressed to Young-Sang Kim or Doo-Jin Kim.